Int. J. Heat Mass Transfer. Vol. 23, pp. 591–608.
Pergamon Press Ltd. 1980. Printed in Great Britain.

TURBULENT FLOW IN A PLANE CHANNEL HAVING ONE OR TWO ROUGH WALLS

L. MEYER
Institut für Neutronenphysik und Reaktortechnik,
Kernforschungszentrum, 75 Karlsruhe, Germany

(*Received* 26 *March* 1979)

Abstract—The assumption of universal velocity profiles over smooth and rough surfaces is widely used in calculations on flow in rough channels. Experiments on fully developed turbulent flow in a rectangular channel with variable aspect ratio were performed to determine the parameters of the velocity profiles over two-dimensional rectangular roughnesses. The pressure and velocity profiles in the fully rough flow regime were measured in channels with one and with two rough walls. The results show that the slopes of the non-dimensional velocity profiles in the smooth and rough zones decrease with the increasing relative roughness, height and drag of the rough wall, contrary to the generally accepted assumption of a constant profile slope. The profile parameters were correlated as functions of the channel- and roughness geometry and were used in a transformation method which was applied to data from experiments on rectangular and annular channels carried out by other investigators.

NOMENCLATURE

- A, slope of the logarithmic velocity profile;
- B, constant of the logarithmic velocity profile at a smooth wall;
- b, width of the roughness rib [m];
- d_h, hydraulic diameter [m];
- E, parameter of the velocity profile at a rough wall;
- F, force upon a roughness rib per unit length [N m^{-1}];
- f, friction factor, $2\tau/\rho u^2$;
- f_0, friction factor of a smooth tube;
- h, height of roughness rib [m];
- h^+, dimensionless height of roughness rib, hu_τ/ν;
- L, width of channel [m];
- l_r, length of eddy downstream of a rib (re-attachment length) [m];
- p, axial pitch of the repeated roughness ribs [m];
- p, pressure [N m^{-2}];
- u, mean velocity [m s^{-1}];
- u_τ, friction velocity, $(\tau/\rho)^{1/2}$ [m s^{-1}];
- u^+, dimensionless velocity, u/u_τ;
- $\bar{u}$, average velocity in a section [m s^{-1}];
- R, parameter of the logarithmic velocity profile at a rough wall;
- Re, Reynolds number, ud_h/ν;
- x, axial distance;
- y, distance normal to the wall;
- y^+, dimensionless distance from the wall, yu_τ/ν;
- $\hat{y}$, position of the zero shear stress line, length of respective zones;
- z, distance parallel to the wall normal to the flow.

Greek symbols

- ε, displacement of the origin of the velocity profile at a rough wall [m];
- ν, kinematic viscosity [m^2 s^{-1}];
- ρ, density [kg m^{-3}];
- τ, shear stress [N m^{-2}].

Subscripts

- m, mean value of a periodic quantity;
- max, maximum;
- dyn, dynamic;
- r, at the rough wall or pertaining to the rough zone;
- s, at the smooth wall or pertaining to the smooth zone;
- st, static;
- vol, volumetric definition of the origin of the velocity profile;
- 01, pertaining to the relative roughness height $h/\hat{y}_r = 0.01$.

1. INTRODUCTION

FULLY developed turbulent flow in rough channels has been studied in numerous experimental investigations, especially since the use of artificial roughnesses to promote heat transfer in gas-cooled nuclear reactors became important. However, there is no general agreement on such basic features as the pressure drop coefficients and the velocity profiles. One of the main problems is that these features vary with a change of channel dimensions at constant roughness geometry. The friction factor (pertaining to the rough wall only) for asymmetrical flow in rough ducts, such as annuli or rod bundles in particular, is difficult to determine due to the unknown position of zero shear stress.

Experiments to determine the thermal performance of certain roughnesses are usually carried out with single rough rods contained in smooth tubes, and the results have to be transformed for rod bundle geometry. The geometry selected for the present study was a rectangular duct of sufficiently large aspect ratio for

the flow along the mid-plane to be treated like the flow between parallel planes, thus simulating an annulus with a radius ratio close to one. A functional relationship between the parameters determining the velocity profile and the friction factor on the one hand, and the geometrical parameters of the roughness and of the channel on the other hand was sought in order to verify or improve existing transformation methods.

2. THEORETICAL BACKGROUND

In the determination of pressure loss Δp in closed channels, or in the evaluation of experiments in tubes or annuli, usually only integral quantities, such as mass flow rates or bulk velocities, are known. The relation between Δp and these quantities is given by

$$\Delta p = f \frac{\rho}{2} \bar{u}^2 \frac{\Delta x}{d_h/4}, \tag{1}$$

where f is the Fanning friction factor.

In order to determine friction coefficients of rough walls from pressure loss experiments in channels having both smooth and rough walls, the respective flow areas must be theoretically separated, the boundary between the areas being taken to be the zero shear stress plane. Two fundamentally different methods are generally used: these may be designated the f-method and the R-method.

2.1. *The* f-*method*

Hall [1] assumed that the zero shear stress line which divides the annular space between a rough rod and an outer smooth tube is coincident with the line of maximum velocity; this position could therefore be determined by velocity measurements. With the respective hydraulic diameters of the inner rough zone and of the outer smooth zone known, the two Reynolds numbers and friction factors could be calculated, and correlations found. Subsequently, Wilkie [2] proposed a simplified method which does not require velocity profile measurements. From measurements in different annuli he found that the friction factor f_s of the outer smooth zone depends on the magnitude of the friction factor f_r of the inner rough zone. He correlated his experimental results in a function K_3,

$$f_s/f_{0s} = K_3(f_r/f_{0r}), \tag{2}$$

where f_0 stands for the theoretical value of the friction factor of a smooth pipe at the relevant Reynolds number. Similarly, he produced a function K_2 for the ratio of the average flow velocities in the two regions of the annulus,

$$\bar{u}_s/\bar{u}_r = K_2(f_r/f_{0r}). \tag{3}$$

When it became clear that the zero shear stress line does not coincide with the position of maximum velocity in asymmetrical flow, Nathan and Pirie [3], and Warburton and Pirie [4] developed Wilkie's method, transforming to the true position of the zero shear. The friction factors of the rough zones are described as functions of the Reynolds number and the ratio of roughness height to hydraulic diameter. By means of these correlations different channel geometries may be treated.

2.2. *The* R-*method*

This method is based on the existence of velocity profiles obeying the 'law of the wall', i.e. at smooth surfaces

$$u_s^+ = A_s \ln y^+ + B \tag{4}$$

and correspondingly at rough walls

$$u_r^+ = A_r \ln y/h + R. \tag{5}$$

In the above equations, u^+ stands for the local streamwise velocity u, normalized by the friction velocity $(\tau_{s,r}/\rho)^{1/2}$, and the subscripts s and r denote whether the rough or smooth wall shear stress, τ_r or τ_s, respectively, is used in the friction velocity. The slope A_r of the logarithmic velocity profile at rough surfaces is generally taken to be the same as that at smooth surfaces with $A_s = 2.5$. Nikuradse [5] has verified this for sand-grain roughnesses but recently there have been some doubts about the value of A_r at artificial roughnesses. This will be discussed later. The roughness height is h, and R is the non-dimensionalized velocity at $y = h$. The parameter R should be characteristic for a certain roughness because it is independent of the Reynolds number at high values of $h^+ = hu_\tau/\nu$.

In order to separate the two zones in asymmetrical flow it is assumed that the zero shear stress plane is given by the intersection of the two velocity profiles originating at the respective walls. Although mathematically the velocity has a maximum at this intersection, Maubauch [6] showed that agreement with the experimentally determined line $\tau = 0$ is good. Integration of equations (4) and (5) over the respective flow areas yields the friction factors and Reynolds numbers. The results are correlated in terms of the roughness parameter R. The assumption that R is a function of only the roughness geometry at high values of h^+ was not, however, confirmed. Experiments evaluated by this method [7–9] have shown that R is also a function of the relative roughness height. The friction factor ratio f_s/f_{0s} of the smooth zone is a weak function of Re_s if this method is applied. In contrast to the results in [2–4] this ratio is almost independent of the friction factor of the rough zone. Dalle Donne [8, 9] developed the R-method in such a way that the data of Warburton and Pirie are taken into account. The slope A_s of the logarithmic velocity profile in the smooth region is altered in an iterative process until Warburton's [10] relation

$$f_s/f_{0s} = K'_3(f_r/f_s) \tag{6}$$

is satisfied. The friction factor of the rough zone differs from the results of the calculation with constant A_s by between -3% and $+1\%$. The dependence of the roughness parameter R on h^+ and on the relative roughness height is changed very little by this modification of the R-method.

Comprehensive comparisons of both methods, including heat transfer, are to be found in references [8, 9].

3. PREVIOUS MEASUREMENTS

3.1. *Velocity distribution*

Reports of velocity profile measurements at rough surfaces are quite numerous but few concern the fully rough regime at an artificial roughness in fully developed turbulent flow in a closed channel. Measurements for free surface flow over a bed composed of hemispheres were performed by Bayazit [11]. He found a strong decrease in A_r when the flow depth was reduced. Because of the different boundary conditions compared to a closed duct, his results cannot be generalized. Investigations of certain two-dimensional roughnesses reported in [12–18] yielded slopes A_r, which deviated from the generally accepted values of $A_r = 2.5$ or $A_r = 2.39$ unless the origin of the velocity profile was taken to be behind the actual wall.

Velocity measurements in pipes internally roughened with square transverse ribs with four different pitch to height ratios at a constant rib height to pipe diameter ratio were performed by Whitehead [19, 20]. In the fully rough flow region, which was reached at h^+ values considerably higher than $h^+ = 70$, the slope A_r was found to be a function of the p/h-ratio.

Baumann [21] has investigated the dependence of A_r on the rib height to channel width ratio h/L for square two-dimensional roughnesses with three different p/h-ratios in a rectangular closed water channel. He found $A_r = 2.55$ for low h/L values, while with increasing rib heights the slope A_r increases or decreases depending on the p/h-ratio of the roughness. Constant values of A_r and R, i.e. independent of the Reynolds number, were obtained at higher values of h^+ with increasing roughness height. In the range $0.01 \leq h/L \leq 0.02$ this occurs approximately when $h^+ \geq 3.2 \times 10^4 (h/L)^{1.33}$.

3.2. *Static pressure*

Due to the turbulent motion, the static pressure away from the wall must be lower than that close to the wall, as can easily be seen from the Reynolds equations. For practical purposes, such as velocity measurements in smooth channels by means of Pitot tubes, this pressure difference may be negligible.

For boundary layer flow in a wind tunnel, Furuya *et al.* [22] have measured the static pressure over wire roughnesses 2 mm in diameter with $p/h = 32$. Almost no variation has been detected axially between the roughnesses, but close to each roughness element the static pressure is low by 1% of the dynamic pressure of the main flow. This local under-pressure diminishes with increasing distance from the rough wall and is zero at $y = 10h$. For square roughnesses with $p/h = 7.2$, Lawn [14] found differences of more than 10% between velocity measurements made by a hot wire anemometer and those made by a Pitot tube together with a static pressure tapping at the opposite smooth wall. He attributed these differences to the static pressure variation in the flow. Only at distances greater than 15 rib heights from the rough wall was no difference in velocity detected. Consequently, all velocity measurements at rough walls made by a Pitot tube with a static pressure measurement at a different position are subject to error.

4. THE EXPERIMENT

4.1. *Apparatus and procedure*

To approximate the flow between infinite parallel plates, a rectangular vertical channel with variable aspect ratio (between 3.3 : 1 and 11.7 : 1) was used (see Fig. 1). The internal dimensions of the channel were: 700 mm in the width direction (z), 60 mm minimum and 210 mm maximum in the y-direction, and 7800 mm in the axial direction (x), with tolerances of ± 0.5 mm. Three of the channel walls were made of Plexiglass, and one wide wall, which was adjustable, was made of aluminum, all were 10 mm thick. Air drawn in through a silencer and filter by a radial blower entered the test section through a honeycomb grid. Measurements were made near the open outlet. Preliminary measurements showed that the flow was fully developed for all aspect ratios. Profiles in the z-direction showed a zone of approximately 100 mm in the middle of the channel in which the influence of the short side walls was negligible. The roughness elements, aluminum ribs with $h = 10$ mm, were fixed to one of the wide walls by double-sided adhesive tape. At

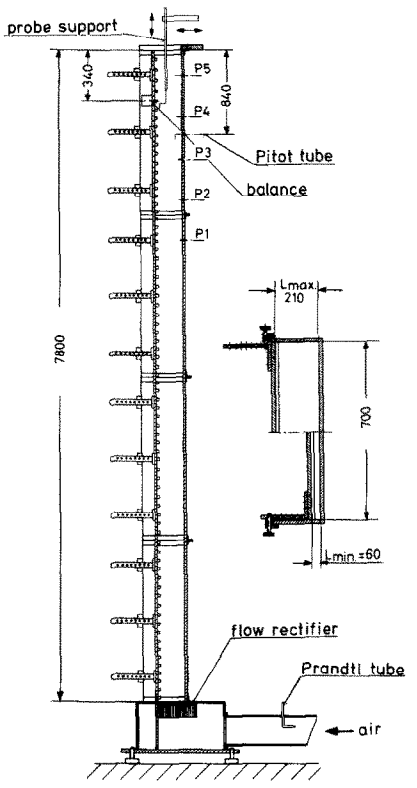

FIG. 1. The test section.

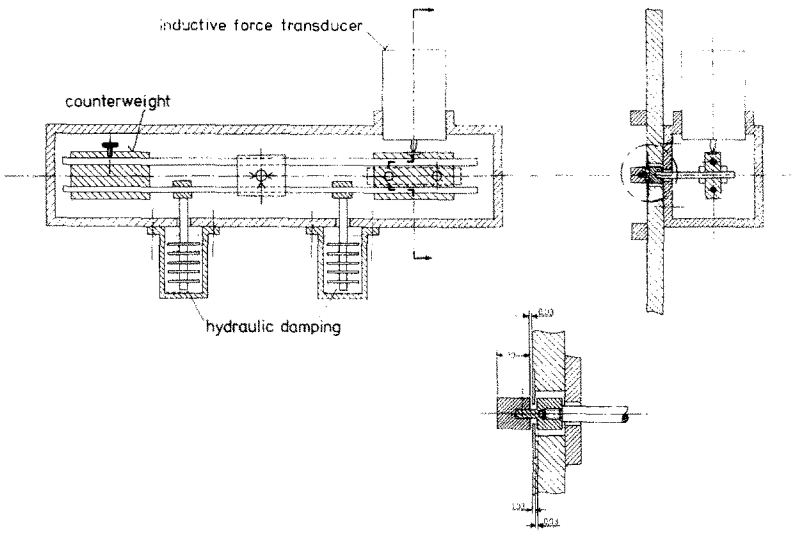

FIG. 2. The force-measuring system.

340 mm upstream of the outlet, a roughness element was connected to a balance which served to measure the force acting upon the rib. The axial pressure drop was measured by five pressure taps in the smooth wall over a length of 2500 mm.

Figure 2 shows a schematic representation of the force-measuring system. The exchangeable rib was attached to a beam whose axis of rotation was normal to the direction of the flow and to the wall (y-direction). It was thus ensured that the point of attack of a force, irrespective of whether this was at the bottom or the top of the rib, did not influence the reading. Since the flow in the region of the measuring rib was a uniform two-dimensional flow, the effect produced by the two different lengths of the lever arm on both sides of the center were automatically offset. The weight of the rib was balanced out by a counterweight. An important requirement was easy mobility of the measuring rib with a minimum leak rate at the bottom of the rib and along the sides. At the bottom, a labyrinth seal with adjustable gap widths of approximately 0.03 mm was created; the gap on the sides was set to approximately 0.03 mm. Preliminary experiments at single ribs with measuring ribs of different lengths gave identical results; hence, influence of the lateral gap could be excluded.

The force measurement, proper, was performed by means of an inductive force transducer with 0.2 mm deflection at full range. The housing of the balance was sealed to make it pressure-tight relative to the external pressure. However, readings with the unsealed balance were no different, which seemed to prove a very low leak rate at the rib. Fluctuations were eliminated by hydraulic damping of the balance beam and by electronic damping. The balance was mounted on an aluminum plate which fitted into the channel wall as an inset. The velocities were measured by means of a circular Pitot tube with an outer diameter of 0.6 mm. The corresponding static pressures were measured with a second tube, axially aligned with the flow direction, and having four holes at its circumference, 90° apart. Since the measurement of static pressure in turbulent flow is problematic, extensive tests of the measuring device were made. Tubes with different diameters ($0.6 \leq d_a \leq 1.5$ mm) and wall thicknesses ($0.15 \leq l_s \leq 0.525$ mm) were tested. The holes had a diameter of $d_s = 0.15$ mm, hence, the length to diameter ratios of the pressure taps were in the range of $1 \leq l_s/d_s \leq 3.5$. The position of the holes with respect to the rough wall was varied also. All variations in the pressure readings were small compared to the difference between the readings of the static pressure tube and a static pressure tap at the smooth wall at the same axial position. So, the tube with the smallest diameter (0.6 mm) was used in order to disturb the flow as little as possible.

In accord with recommendations for the design of static tubes [23], the head was ellipsoid-shaped and the holes were more than 10 tube diameters away from the tip. The lateral distance between the static tube and the Pitot tube could be varied and was set to 10 mm: tests had shown that the tubes influenced each other when they were less than 3 mm apart. In measurements close to the smooth wall, there was no difference between the readings of the static tube and the static pressure tap in the wall, up to about 2 mm from the wall. For measurements closer than that, especially for the determination of the smooth wall shear stress by the Preston method, the static tube was positioned about 2 mm away from the wall. The cross slide, which could be used to position the probe with an accuracy of 0.01 mm at any position of the flow cross-section, was installed 15 cm downstream of the channel outlet in order not to block the flow.

To minimize disturbances to the flow, the probe support had to be thin but for suppression of vib-

Table 1. Geometrical parameters

b/h	p/h	L/h
1	4	6, 8.5, 13.5, 21
1	8	6, 8.5, 13.5, 21
1	16	6, 8.5, 13.5, 21
1	32	8.5, 21
2	8	6, 8.5, 13.5, 21
1	8	11, 21 both walls rough

rations, a certain rigidity was necessary. The probe support had a diameter of 4 mm at its end and extended up to 600 mm into the channel, i.e. measurements were possible up to 260 mm upstream of the force-measuring rib.

4.2. *Test parameters*

Five different roughnesses were investigated. The height of all roughnesses was $h = 10.4$ mm (10 mm aluminum + 0.4 mm adhesive tape). The channel width L was changed up to four times for each roughness. Table 1 shows the geometrical parameters obtained with $h = 10$ mm.

At least four different mass flow rates were used for each roughness and channel width. Minimum air velocity was 12 m s^{-1}, maximum was 45 m s^{-1}, which resulted in a Reynolds number range of $10^5 < Re < 6 \times 10^5$. The values of h^+ ranged between 800 and 3000.

5. EVALUATION

5.1. *Velocity*

The time mean velocity u was calculated from the differential pressure between the Pitot tube and the static tube, and the density of the humid air. The position of the Pitot tube near the smooth wall was corrected for according to MacMillan [24]. However, the velocities were not corrected for the effect of turbulence: turbulence intensities at rough walls are not known, and the effect of turbulence, especially on the static pressure reading, is not known. The opinions of different authors about this are highly controversial: Goldstein [25] states that the readings of both tubes are higher by an additive factor $c\rho\overline{q'^2}$, with q' being the resultant turbulent velocity and the value of c for the total head being $c = 1/2$ while for the static pressure $c = 1/6$, if the turbulence is isotropic. Hinze [26] states that, because of velocities normal to the static tube, the pressure reading is too low with $c = -1/2$. Becker and Brown [27] give correction formulae for total head probes, which depend on the probe geometry and turbulence intensity. The correction for small tube diameter is negligible.

5.2. *Wall shear stresses*

The shear stress at the smooth wall was determined by Preston tubes using the Patel [28] calibration. The shear stress at the rough wall could be determined in two ways. The first method is based on knowledge of

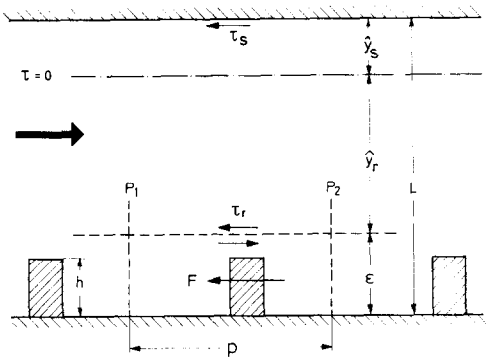

FIG. 3. Scheme of the flow cross-section.

the axial pressure drop dp/dx and the shear stress at the smooth wall τ_s. Since there is a region in the center of the channel, in which the influence of the short side walls on the flow is negligible, a force balance for steady flow yields

$$(\tau_s + \tau_r)dz\,dx = L\,dz\,dp. \tag{7}$$

Because of the discrete roughnesses, the average over at least one pitch must be taken, thus the mean shear stress is

$$\tau_r = L\frac{\Delta p}{\Delta x} - \tau_s. \tag{8}$$

The reference surface for this shear stress is the smooth wall between the ribs ($\varepsilon = 0$, see Fig. 3). With another reference surface ($\varepsilon \neq 0$), τ_r changes to

$$\tau_r = (L - \varepsilon)\frac{\Delta p}{\Delta x} - \tau_s. \tag{9}$$

The second method of determining the shear stress at the rough wall is based on the measurement of the force acting upon that wall. Lavallee and Popovich [29] showed that the negative and positive portions of the shear stress due to viscosity at the smooth wall between the ribs cancel each other out for square roughnesses with $p/h = 12.5$. From other measurements [30, 31] it is known that for roughnesses with $p/h = 16$ the error is less than 3%, if only the force acting upon the rib is considered in the determination of the total stress. For pitch to height ratios of $p/h = 32$, the error can rise up to 10%.

A force balance over the control volume with the length p and the height ε yields

$$F = \tau_r p + (p_1 - p_2)\varepsilon. \tag{10}$$

Pressure patterns along the boundary of two successive grooves are assumed to be similar. From equation (10) the shear stress can be found thus

$$\tau_r = \frac{F}{P} - \frac{\Delta p}{\Delta x}\varepsilon. \tag{11}$$

The dependence of τ_r on the choice of the reference surface ε is the same in equations (9) and (11).

5.3. *The position of zero shear* ($\tau = 0$)

The lengths $\hat{y}_s$ and $\hat{y}_r$ of the zones influenced by the smooth and rough walls, respectively, are given by the ratio of the wall shear stresses

$$\frac{\hat{y}_s}{\hat{y}_r} = \frac{\tau_s}{\tau_r}. \tag{12}$$

With $\hat{y}_s = L - \hat{y}_r - \varepsilon$, the length of the 'rough' velocity profile is given by

$$\hat{y}_r = \frac{L - \varepsilon}{1 + \tau_s/\tau_r}. \tag{13}$$

It can be seen that the position of zero shear, however, is not dependent on ε if it is defined by $\hat{y}_s$. From equations (8) and (14) we get

$$\hat{y}_s = \frac{\tau_s}{\Delta p/\Delta x}. \tag{14}$$

6. EXPERIMENTAL RESULTS

6.1. *Outlet effect*

The axial pressure gradient near the outlet of the channel was measured at different y-positions (distance from the rough or smooth wall, appropriately) for different channel widths. At the axial position 1.5 L upstream of the outlet, a deviation from the otherwise linear pressure drop became evident. The pressure drop close to the smooth wall was higher than the linear value, while in the rest of the channel it was lower. This fact was confirmed by measurements of the static pressure across the channel at different axial positions. Consequently, measurements with Pitot tubes in rough channels should be performed at least 1.5 channel widths upstream and not at the outlet.

6.2. *Axial pressure and velocity variation*

Figure 4 shows the influence of the ribs on pressure and velocity at different distances from the wall. The periodic variations of both quantities over one pitch decrease with increasing distance from the rough wall. The velocity reaches its maximum above a rib, while the pressure has its minimum there. The error due to curvature of the streamlines can be estimated to be very low and is not the cause of the pressure and velocity distributions found. The distributions for different p/h- and L/h-ratios look similar, but the magnitude of the periodic variations increases with higher p/h-ratios. The velocity one rib height above the rib tip varies up to $\pm 10\%$ for $p/h = 16$ and even more for $p/h = 32$, irrespective of the channel width L/h. The variation of the maximum velocity increases with lower L/h-ratios; it varies by $\pm 2\%$ for wide channels and up to $\pm 4\%$ for narrow ones.

For large p/h and narrow channels, the shear stress at the smooth wall, which is determined by Preston tube, also varies. Figure 5 shows the variation of τ_s normalized by the average shear stress for different channel widths. For $L/h = 8.2$ the variation is about 10% for $p/h = 16$, and about 30% for $p/h = 32$. There are two positions, where the mean shear stress can be measured: at $x/p = 0.31$ and $x/p = 0.88$, irrespective of the pitch. The mean velocities can be measured at approximately the same axial positions, although the exact positions vary slightly with distance from the rough wall.

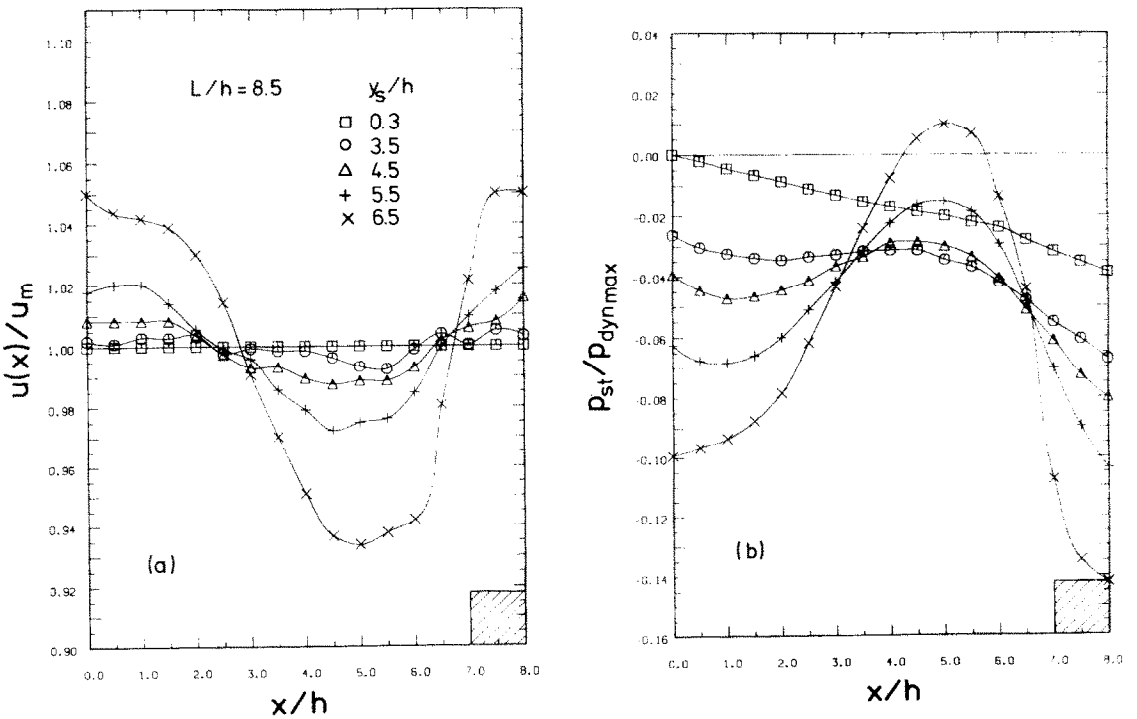

FIG. 4. Axial variation of (a) velocity and (b) static pressure at square roughnesses, $p/h = 7.7$, $L/h = 8.2$.

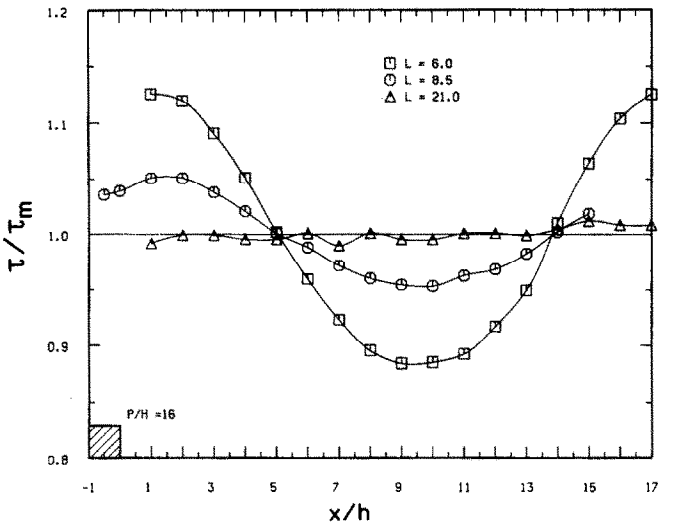

FIG. 5. Axial variation of the shear stress at the smooth wall for different channel widths with a roughness of $p/h = 16$ at the opposite wall.

6.3. *Static pressure distribution normal to the wall*

The static pressure distribution normal to the rough wall is shown in Fig. 6 for a square roughness with $p/h = 3.85$ and $L/h = 8.2$. The static pressure in the flow is generally lower than that at the smooth wall, independent of the axial position, but close to the rough wall (up to a distance $y_r = 2.5\,h$) the pressure is strongly dependent on the position.

The low static pressure in the flow is due to the turbulent motion. From the Reynolds equations, we find that the difference between the pressure at the smooth wall and that within the flow is given by,

$$\Delta p/\rho = \overline{v'^2},$$

while the turbulent stress is given by

$$\tau = -\rho\overline{u'v'},$$

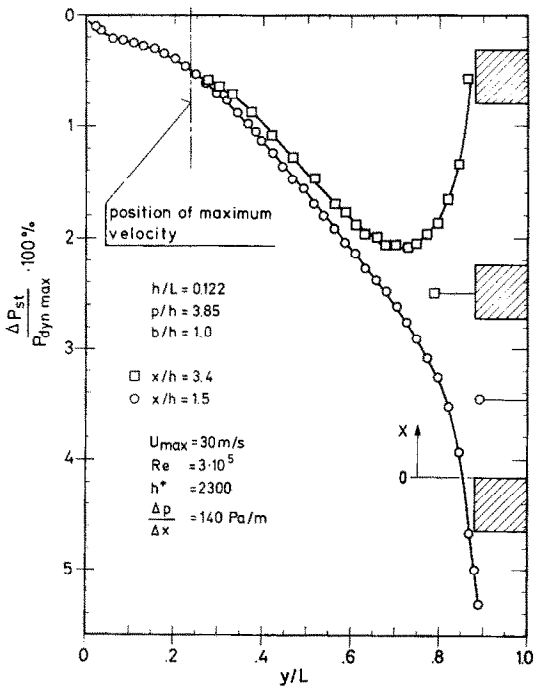

FIG. 6. Static pressure distribution normal to the rough wall.

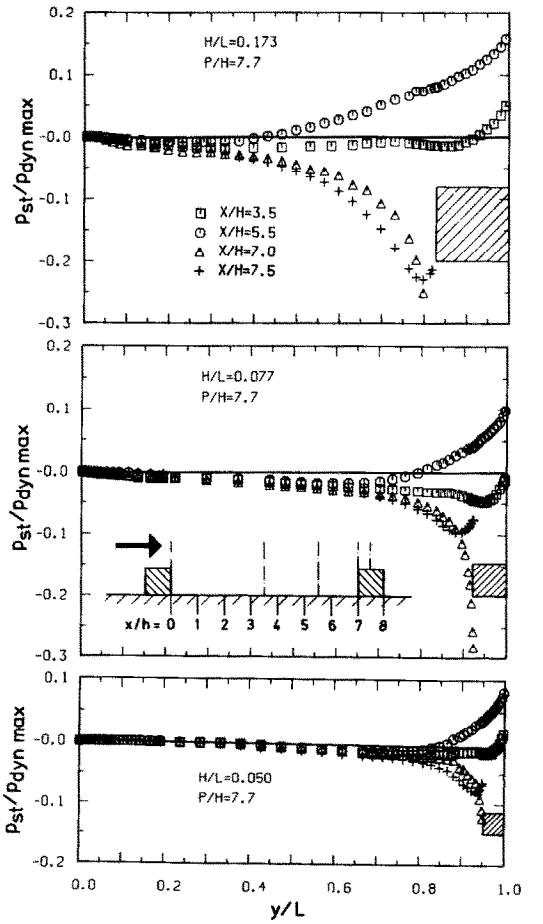

FIG. 7. Static pressure distribution normal to the rough wall.

the viscous stress being neglected. If we compare the friction velocity u_{τ_r}, evaluated from the shear stress at the rough wall τ_r, with the respective turbulent velocity v', evaluated from the difference in the static pressure (approximately 2% of the maximum dynamic pressure for $p/h = 3.85$ in Fig. 6), we find good agreement for all roughnesses.

Another example is shown in Fig. 7 for a square roughness with $p/h = 7.7$ for different axial positions and channel widths. These results agree well with the findings of Furuja *et al.* [22] and Lawn [14].

6.4. *Velocity profiles*

The respective velocity distributions in a channel with one rough wall and with two rough walls are compared in Fig. 8. The effect of the different traversing positions can be clearly seen, although this effect is more pronounced for roughnesses with larger pitch.

In Fig. 9 the mean velocity profiles near the smooth surface are plotted in universal co-ordinates. The shear stress used in determining u_s^+ is an average taken over one pitch. These profiles show the typical characteristics of universal profiles in smooth channels. There is

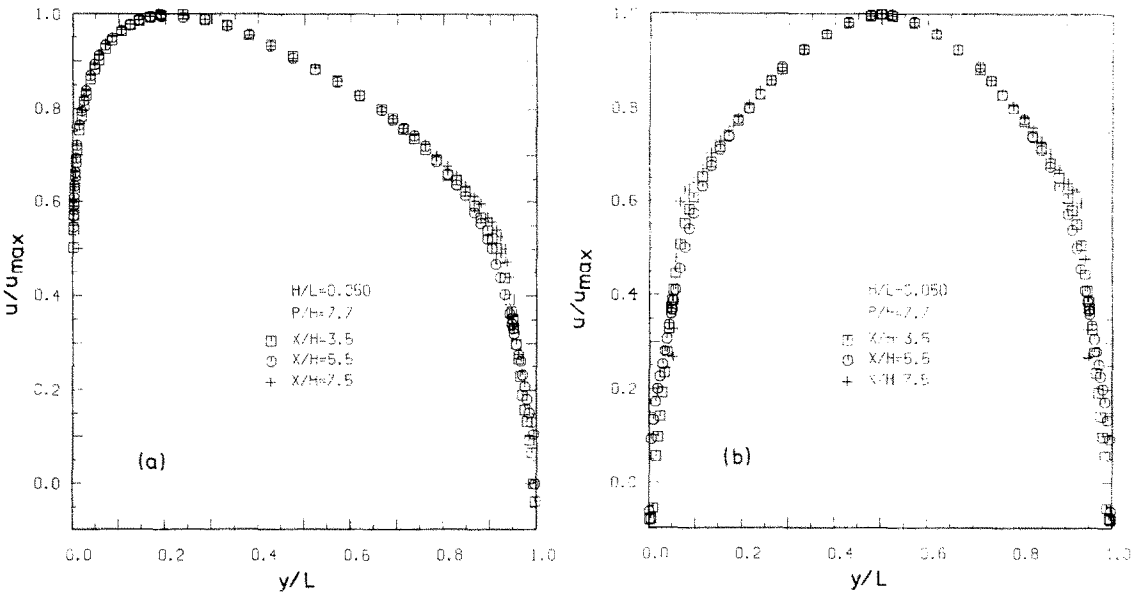

FIG. 8. Velocity profile in a channel having (a) one and (b) two rough walls.

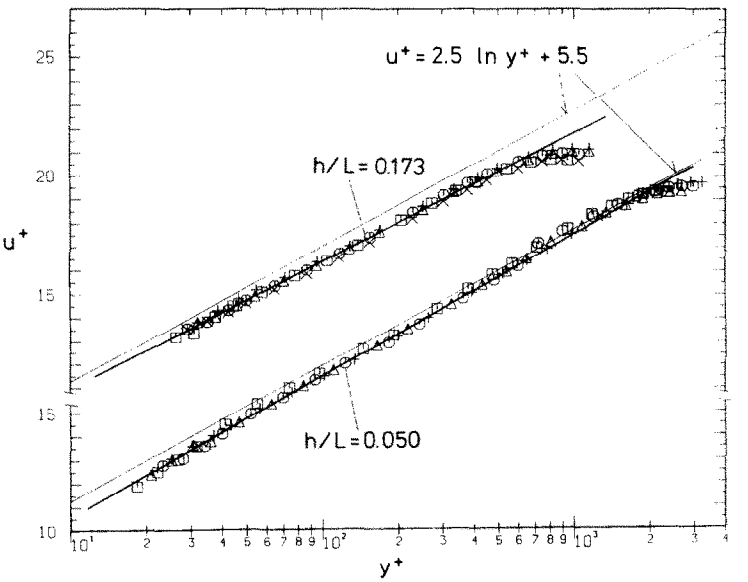

FIG. 9. Non-dimensional smooth-wall velocity profiles for different channel widths with a roughness of $p/h = 3.8$ at the opposite wall.

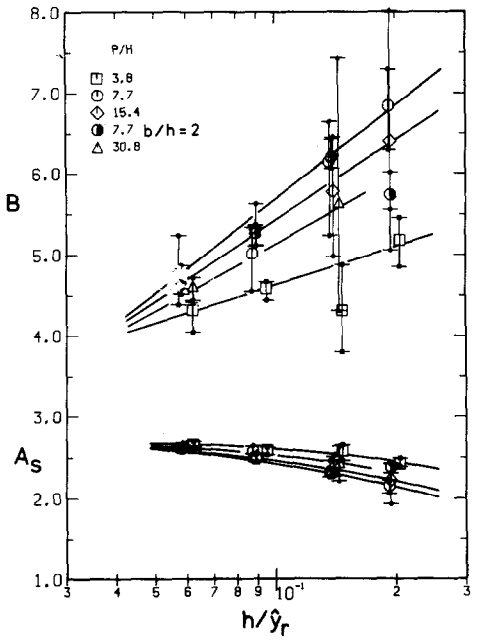

FIG. 10. Variation of parameters of the smooth-wall profile with different roughnesses at the opposite wall.

no Reynolds number effect but a distinct effect due to the rough surface opposite. The slope A_s, together with the constant B, varies with the relative roughness height h/L: with increasing roughness height the slope A_s decreases and B increases. This effect is slightly stronger for roughnesses with higher friction factors ($p/h = 7.7$). The parameters A_s and B also vary with the axial measuring position in relation to the rib position; for larger p/h-ratios this variation is greater, especially for narrow channels, irrespective of whether the local shear stress or an average over one pitch is taken. As mentioned before, the wall shear stress was determined by the Preston method with the constant $A_s = 2.39$ and $B = 5.45$. If the measured velocity profiles show different values for these constants, the determination of the wall shear stress must be incorrect. However, the error involved is estimated to be small, since most Preston measurements lie at $y^+ < 30$ where the influence of the rough wall upon the velocity profile is probably very small.

The parameters A_s and B of all measured profiles were determined by a best fit method, with points for $y^+ < 70$ and those close to the maximum which do not fall upon a straight line being neglected. The mean values of A_s and B for each roughness and channel width combination are shown in Fig. 10 as functions of the relative roughness height, together with the variation due to different axial measuring positions. With one exception the curves follow the trend described above.

The value of the shear stress at the rough wall, determined from the pressure drop and shear stress at the smooth wall by equation (9), and the value obtained from the force measurement at the rib by equation (11), differed by less than $\pm 5\%$. For the evaluation of the friction velocity u_τ, the average of both was used. Figures 11–13 show the non-dimensional velocity profiles at the rough wall for three roughnesses at the lowest and highest h/L-ratios for each. The origin of the profiles is defined volumetrically, i.e. $\varepsilon = hb/p$. There is no Reynolds number effect, which means that the flow was in the fully rough regime. The slope A_r and the roughness parameter R vary with the roughness geometry and relative roughness height: with increasing pitch and relative roughness height, A_r and R depend more and more on the axial position. A compilation of the profile parameters is shown in Fig. 14, where the mean values of A_r and R, determined by a best fit of the points lying on a straight line, and their variation due to the measuring position are plotted against the ratio of the rib height h to the length of the rough profile $\hat{y}_r$. The dependence of the rough profile parameters on the relative roughness height is similar to that of the smooth zone parameters. The roughness parameter R increases with growing relative roughness height. The slope A_r of the logarithmic profile is generally less than 2.5 and decreases with

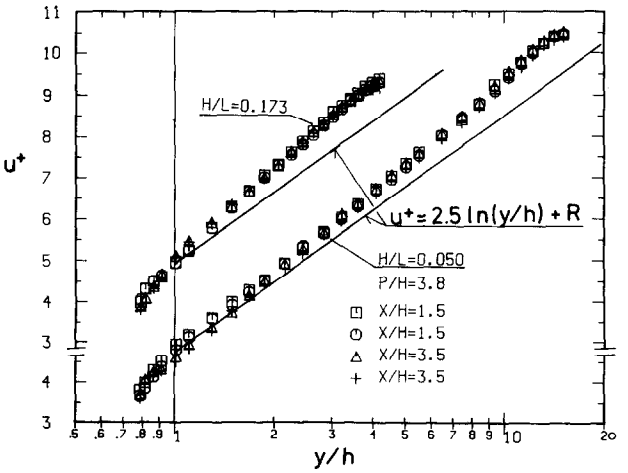

FIG. 11. Non-dimensional rough-wall velocity profiles at different axial positions, $p/h = 3.8$.

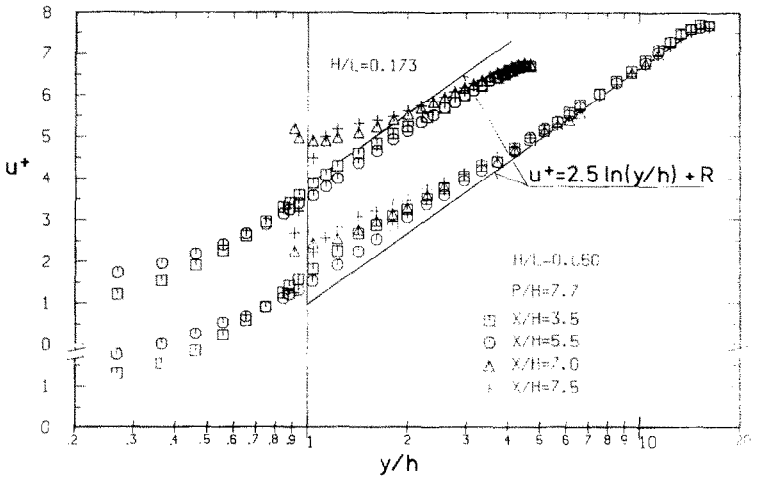

FIG. 12. Non-dimensional rough-wall velocity profiles at different axial positions, $p/h = 7.7$.

increasing relative roughness height, except for the roughness with $p/h = 3.8$; here A_r is greater than 2.5 and increases with higher $h/\hat{y}_r$. Baumann's [21] results for similar roughnesses show the same trends, although there are some doubts about the validity of his results for high $h/\hat{y}_r$-ratios because of the undefined axial traversing position.

One important finding from the present measurements is that A_r and R do not differ for asymmetric and symmetric flow at the same $h/\hat{y}_r$-ratio. The values of A_r and R, however, depend very much on the choice of origin for the velocity profile: a common definition is $\varepsilon = 0$ i.e. at the root of the ribs. Although for high p/h-ratios, A_r and R are not much affected by the definition, for $p/h = 3.8$ A_r rises by approximately 0.25 and R falls by 0.5 compared with the values obtained when the origin is volumetrically defined. The dependence on $h/\hat{y}_r$ is similar.

Rough velocity profiles can be described by choosing the origin in such a way that $A_r = 2.5$ or $A_r = 2.39$: this approach is frequently found in the literature. The parameter ε influences A_r in two ways. Firstly, with decreasing ε the slope A_r in the logarithmic diagram increases and vice versa. Secondly, the shear stress at the rough wall depends on the choice of the reference surface as was shown above, so if ε is reduced, the apparent shear stress increases and the slope A_r decreases. This second influence is counter to the first but much weaker.

In the evaluation of the present measurements, the surface $\varepsilon = 0$ was taken as the reference for the wall shear stress, while for the origin of the velocity profile, ε was changed iteratively until the best fit gave $A_r = 2.5$. Figure 15 shows the variation in the resulting ε, normalized by the rib height h, and in the corresponding roughness parameter R with $h/\hat{y}_r$. The dashed lines

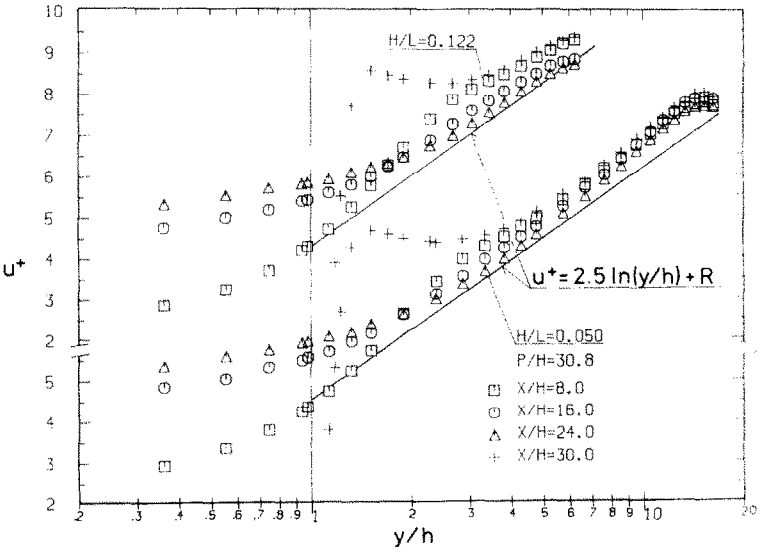

FIG. 13. Non-dimensional rough-wall velocity profiles at different axial positions, $p/h = 30.8$.

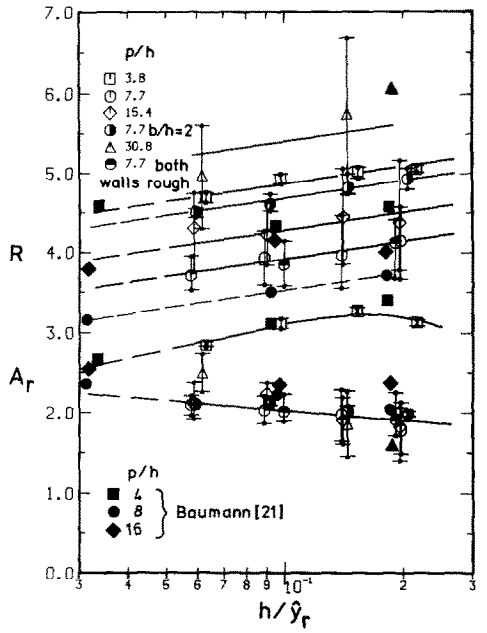

FIG. 14. Parameters A_r and R of the rough-wall profile with a volumetric definition of the origin of the velocity profile.

in Fig. 15 show the results when the origin of the velocity profile is taken as the reference surface for the wall shear stress. Except for the roughness with $p/h = 3.8$ the origin lies below the root of the rib. For $p/h = 3.8$ it is $\varepsilon/h = 0.8$, while for the other square roughnesses the mean value is $\varepsilon/h = -0.75$. Table 2 shows results from the literature.

The discrepancy between the first three authors in the Table is easily understood since the velocity profile depends on the axial position. The measurements of Perry and Joubert [15] were performed in a wind tunnel, and the wall shear stress was determined by putting a straight line through measured points and assuming a slope of $A_r = 2.44$, which is not a reliable method.

Now, there are two ways to describe the velocity profile at a rough wall in terms of the law of the wall. Either the slope A_r is assumed to be constant and a new variable ε is defined, or the origin of the velocity profile is defined in a certain way and A_r becomes a function of the roughness and channel geometry. Besides considerations about the turbulence structures, which might favor one of the two ways, only practical reasons should decide which description is to be used. Since integral quantities are necessary to calculate the flow in a channel, this problem will be discussed later.

7. ANALYSIS OF INTEGRAL QUANTITIES

7.1. *Friction factors*

Friction factors of the rough and smooth zones were determined by numerical integration of the velocities between the respective walls and the zero shear stress line. At the rough wall the integration started at the rib tip or at the root, depending on the measuring position. From the appropriate bulk velocity and the corresponding wall shear stress, the friction factor can be calculated thus

$$\bar{u}_{r,s}^{+} = \frac{\bar{u}_{r,s}}{(\tau_{r,s}/\rho)^{1/2}}, \tag{15}$$

$$f_{r,s} = 2/\bar{u}_{r,s}^{+2}. \tag{16}$$

The Reynolds numbers are given by

$$Re_{r,s} = \frac{\bar{u}_{r,s} 4\hat{y}_{r,s}}{\nu}. \tag{17}$$

The theoretical friction factor of a smooth pipe at the same Reynolds number as that of the smooth or rough zone was calculated by the Prandtl–Nikuradse equation

$$1/f_{0r,s}^{1/2} = 4\log(Re_{r,s} f_{0r,s}^{1/2}) - 0{,}4. \tag{18}$$

Figure 16 shows the friction factor of the smooth zone f_s, normalized by the smooth pipe friction factor f_{0s}, as a function of the ratio f_r/f_s. The origin ε of the velocity profile was defined volumetrically however there would be no fundamental change in the picture with a different definition of ε. The correlation is not very satisfactory and it does not change if the ratio f_r/f_{0r}

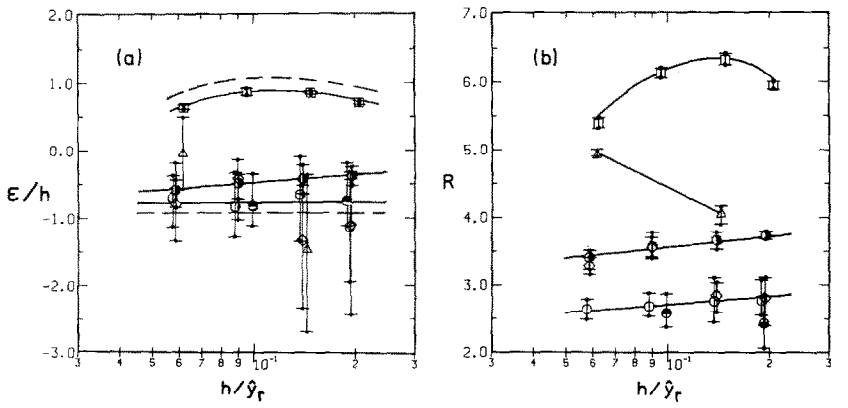

FIG. 15. Displacement of (a) the origin ε of the velocity profile and (b) the roughness parameter R, if $A_r = 2.5$ is pre-set (symbols from Fig. 14).

Table 2. Position of the origin of the velocity profile at rough surfaces

Author	p/h	A_r	ε/h
Hanjalic and Launder [12]	10	2.38	−0.4
Lawn [14]	7.2	2.39	−1.0
Aytekin and Berger [18]	7.2	2.40	−0.2/−0.46
Perry and Joubert [15]	4.0	2.44	0.25

is taken as abscissa. There is, however, an increase in the smooth friction factor ratio with the increasing friction factor of the rough wall. A better correlation exists between f_s/f_{0s} and the geometry parameter h/L or $h/\hat{y}_r$. Although this functional relationship seemed to fit quite well, it was seen in later experiments that it does not hold for roughnesses, such as three-dimensional ones, with higher friction factors. It is easily understood that a mere geometrical parameter cannot describe the full range of potential roughnesses. The frictional characteristics of a roughness are taken into account by the parameter $h/\hat{y}_s$ since $\hat{y}_s$ decreases with higher friction at the rough wall. Figure 17 shows f_s/f_{0s} as a function of this parameter. This relationship can be described by

$$\frac{f_s}{f_{0s}} = 1.056 + 0.0062\frac{h}{\hat{y}_s}, \tag{19}$$

which accommodates three-dimensional roughnesses. This correlation is the only one which is independent of the parameter ε.

7.2. *Profile parameters*

For the development of a transformation method (R-method) based on the present measurements, the following points are crucial:

(i) The position of the line $\tau = 0$ averaged over one pitch is independent of the parameter ε.

(ii) If the profile parameters A_s, B, A_r and R are determined by a best fit in a semi-logarithmic plot, the intersection of the two resulting functions does not give the zero shear stress line. This was verified by calculation. It is, however, possible to choose ε in such a way that the velocity profiles intersect at the line $\tau = 0$.

(iii) Integration of equations (4) and (5) with the profile parameters determined by the best-fit method does not yield the true bulk velocity because the velocity departs too much from a semi-logarithmic straight line.

Hence, for a consistent determination of profile parameters the following conditions must be met:

$$\bar{u}_s = \frac{u_{\tau s}}{\hat{y}_s}, \quad \int_0^{\hat{y}_s} f(A_s, B)\mathrm{d}y, \tag{20}$$

$$\bar{u}_s = \frac{u_{\tau r}}{\hat{y}_r}, \quad \int_0^{\hat{y}_s} f(A_r, R)\mathrm{d}y, \tag{21}$$

$$u_{s\max} = u_{r\max}. \tag{22}$$

If we use the law of the wall [equations (4) and (5)] to describe the flow in a plane channel, the above conditions may be written

$$\bar{u}_s = u_{\tau s}\left[A_s \ln\left(\frac{\hat{y}_s u_{\tau s}}{\nu}\right) + B - A_s\right], \tag{23}$$

$$\bar{u}_r = u_{\tau r}\left[A_r \ln\left(\frac{\hat{y}_r}{h}\right) + R - A_r\right], \tag{24}$$

$$\left[A_s \ln\left(\frac{\hat{y}_s u_{\tau s}}{\nu}\right) + B\right]u_{\tau s} = \left[A_r \ln\left(\frac{\hat{y}_r}{h}\right) + R\right]u_{\tau r}, \tag{25}$$

with

$$\hat{y}_r = L - \varepsilon - \hat{y}_s.$$

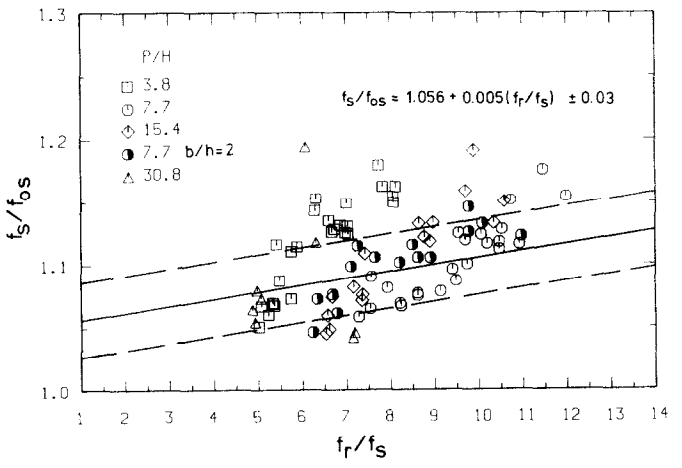

FIG. 16. Variation of the friction factor of the smooth zone f_s with the friction factor of the rough zone f_r.

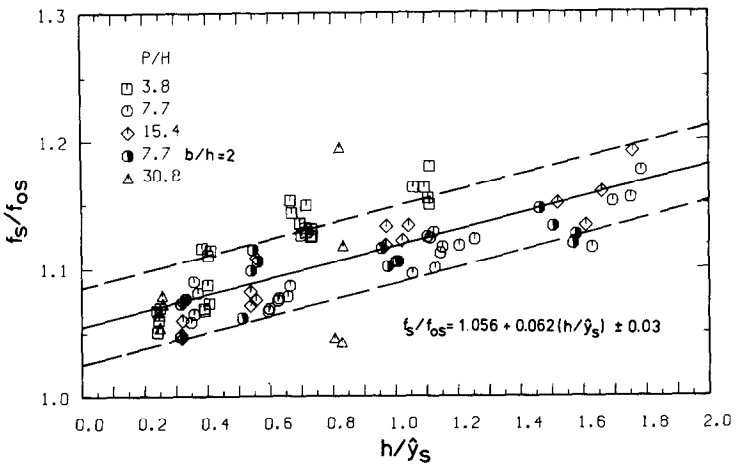

FIG. 17. Variation of the friction factor of the smooth zone f_s with the relative length of the smooth zone.

Of the five variables, A_s, B, A_r, R, and ε, two must be preset, while the other three are determined by equations (23), (24), and (25). The criteria for a choice of the two variables to be preset are: easy resulting correlations for all five variables, and similarity to the variables which were determined by the best fit of the semi-logarithmic straight line in the velocity profile. Presetting the parameters ε and B has turned out to be most suitable. Another interesting choice would be to set $A_r = 2.5$, $\varepsilon = \varepsilon_{vol}$ or $B = 5.5$, as this would correspond to the method currently used: setting A_r, ε, and B at the same time is not possible because of the redundancy in determination, while setting $A_r = 2.5$ and $\varepsilon = \varepsilon_{vol}$ results in unrealistic values for A_s and B, so methods using these parameters would yield incorrect results.

If one of the parameters in the 'smooth' profile is chosen, the other one is determined independently of the parameters in the 'rough' profile. For $B = 5.5$ the resulting values of A_s are shown in Fig. 18. Except for the large pitch roughness ($p/h = 30.8$), the variation in A_s due to different measuring positions is negligible. The data can be correlated by the expression

$$A_s = 2.60 - 0.1 \ln\left(\frac{h/\hat{y}_r}{0.01}\right). \tag{26}$$

As in the friction factor results, the data for three-dimensional roughnesses do not fit into the correlation: the decrease in A_s with increasing $h/\hat{y}_r$ was greater than that found for two-dimensional roughnesses. By considerations analogous to those which led to equation (19), a correlation was found for A_s, which holds for roughnesses with higher friction, [Fig. 18(b)]:

$$A_s = A_{s0} + \frac{0.4}{\ln(0.1\, h/\hat{y}_s)}. \tag{27}$$

For small ratios of $h/\hat{y}_s$, the slope A_s takes the value $A_{s0} = 2.55$. This constant might be a weak function of the Reynolds number, but this could not be verified by the present investigation.

If the slope of the rough profile is taken to be $A_r = 2.5$, the resulting values for the parameter ε are dependent on the roughness geometry and channel width in a way similar to that shown in Fig. 15 (for a table of results see [30]). Since negative values of ε complicate the calculation of the flow in rough channels, a variable slope A_r is preferred.

An illustration of the effect of ε on the parameters A_r and R is given in Fig. 19(a) for $\varepsilon = 0$, and in Fig. 19(b) for $\varepsilon = h$. There is a large disparity in R between the two cases and the variation of A_r with $h/\hat{y}_r$ is also quite different. With a volumetric definition of ε, the trends in A_r and R look similar to those for $\varepsilon = 0$. Extrapolation to small relative roughness heights gives a slope of $A_r = 2.5$ for all roughnesses with $\varepsilon = 0$. A possible function $A_r = f(h/\hat{y}_r, p/h)$ has the drawback that the transition from roughnesses with small p/h-ratios to a smooth wall ($p/h \to 0$) is inconsistent. This is not so if $\varepsilon = h$. However, in this case, extrapolation to small $h/\hat{y}_r$-ratios yields slopes of $A_r > 2.5$, which are also inconsistent. Hence, there is no sensible correlation for A_r with a constant ε for all roughnesses. A volumetric definition of the common type does not

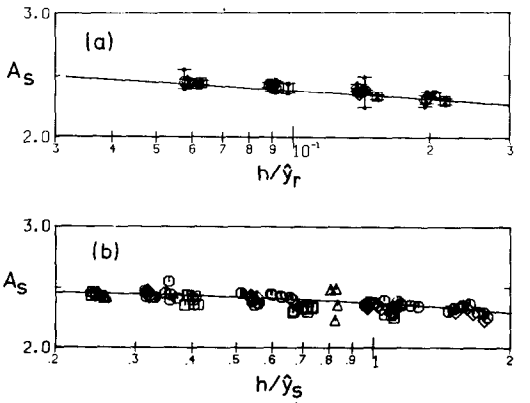

FIG. 18. The profile parameter A_s calculated by equation (23) with $B = 5.5$, (a) as a function of $h/\hat{y}_r$ and (b) as a function of $h/\hat{y}_s$. (Symbols from Fig. 10.)

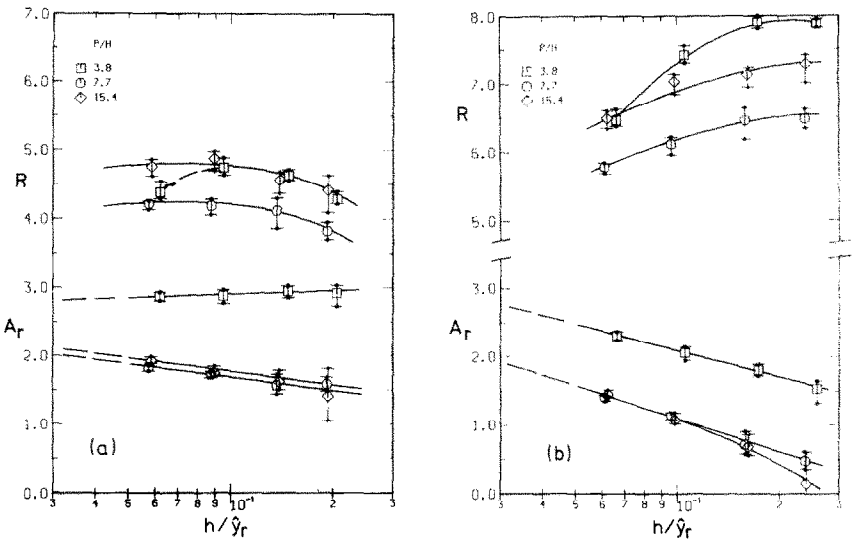

FIG. 19. Parameters of the rough-wall profile calculated by equations (24) and (25) using different definitions of the origin of the profile: (a) $\varepsilon = 0$; (b) $\varepsilon = h$.

afford any improvement. Therefore, a different volumetric definition is proposed.

With reference to the flow behaviour at the ribs, an eddy of length l_r is assumed (see Fig. 20). If this eddy zone is regarded as solid, a volumetric definition yields

$$\left.\begin{aligned} \frac{\varepsilon}{h} &= \frac{2b + l_r}{2p} && \text{for } l_r \le p - b, \\ \text{and} & \\ \frac{\varepsilon}{h} &= 1 - \frac{(p-b)^2}{2p\,l_r} && \text{for } l_r > p - b. \end{aligned}\right\} \quad (28)$$

The length l_r determines the variation of ε as a function of the p/h-ratio. Compared with the common volumetric definition, ε approaches the value $\varepsilon = h$ faster with decreasing p/h-ratios. For $l_r/h = 3$, the resulting A_r functions are plotted in Fig. 21. This value of l_r gives rise to the best functions for A_r and lies between the measured value of $l_r/h = 4$ for $b/h = 1$, and $l_r/h = 2.4$ for $b/h = 2$ [30, 31]. All values of A_r are below 2.5 and approach the value $A_r = 2.5$ with decreasing $h/\hat{y}_r$. The measurements are best approximated by the relation

$$A_r = 2.5 + \frac{E}{\ln(h/\hat{y}_r)}, \quad (29)$$

with

$$\left.\begin{aligned} E &= 2.3 - 0.026\frac{p-b}{h} && \text{for } \frac{p-b}{h} \ge 7. \\ \text{and} & \\ E &= -0.6 + 0.388\frac{p-b}{h} && \text{for } \frac{p-b}{h} \le 7. \end{aligned}\right\} \quad (30)$$

The parameter E is a measure of the deviation of the slope of a rough profile from that of a smooth profile;

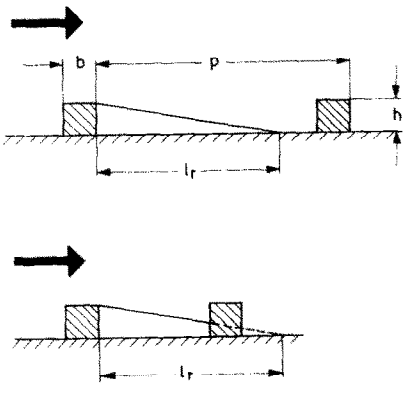

FIG. 20. Approximate flow model for the definition of the origin of the velocity profile.

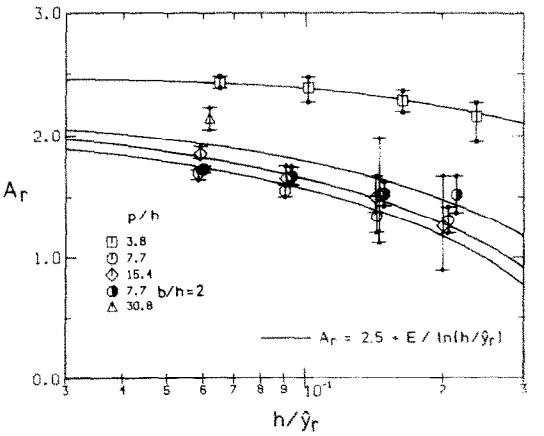

FIG. 21. The profile parameter A_r calculated by equations (24) and (25) using a quasi-volumetric definition (28) of the origin of the velocity profile.

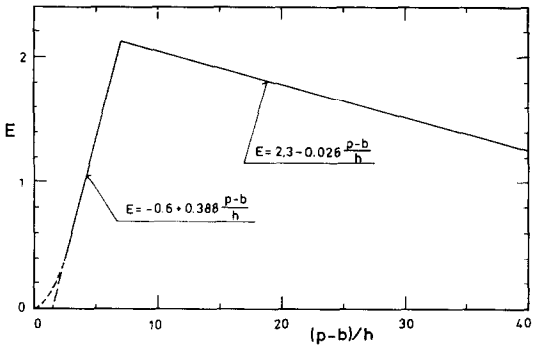

FIG. 22. The parameter E.

the function is shown in Fig. 22. It is evident that there is a proportionality between E and the friction coefficient of a roughness: the parameter E is high for roughnesses with high friction and a low roughness parameter R, but it decreases to zero, i.e. $A_r = 2.5$, if the roughness is weak. The expressions (30) for E can certainly be improved, especially for roughnesses that are not square, if more data are available.

8. APPLICATION OF THE TRANSFORMATION METHOD

Equations (27)–(30) give the slopes of the velocity profiles in the smooth and rough zones of an asymmetrical rough channel as functions of the ratios p/h and L/h. With a knowledge of the slopes A_s and A_r, and the constant B in the smooth profile, measurements can be evaluated when only the friction factor and the Reynolds number of the whole channel are known. Friction factors for the rough and smooth zones and the roughness parameter R can be determined (for a derivation of the requisite equations, which are based on equations (23)–(25), see [30] for parallel plates, and [6] for annuli).

8.1. *Parallel-plate channels*

The present experiments and those experiments performed in a rectangular water channel by Baumann [21] were evaluated by taking the total friction factor and Reynolds number and the geometrical parameters as input data. The resulting values of R are shown in Fig. 23. Only four runs, each performed at the highest Reynolds number, were taken from [21] except for the case with $p/h = 8$ and $h/\hat{y}_r = 0.01$, where only one run was available at a sufficiently high Reynolds number for the fully rough flow regime to prevail.

Although the p/h- and b/h-ratios in the present experiments and those in Baumann's work differed only slightly, the total friction factors for $p/h = 8$ and $p/h = 16$ at the same $h/\hat{y}_r$-ratios differed by up to 10%, hence the different values of R for similar roughnesses. The differences between values of the friction factor of the rough zone calculated by the present transformation method and the experimentally determined values were less than 0.1% for the mean error, and less than 0.5% for the standard deviation in both sets of

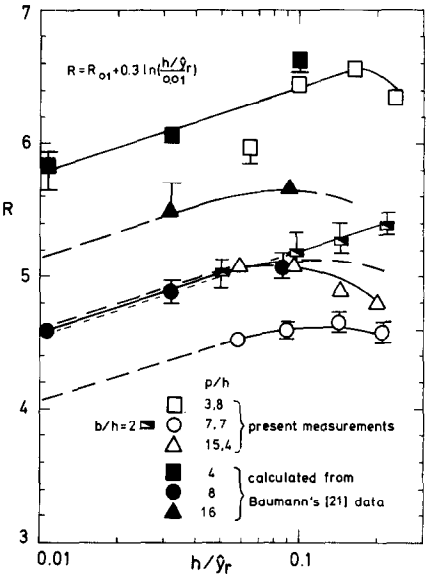

FIG. 23. The roughness parameter R in plane channels.

experiments. This is proof of the accurate determination of the zero shear stress line by the use of equations (27)–(30). By combining the results of both sets of experiments, the following relation for the parameter R can be obtained from Fig. 23:

$$R = R_{01} + 0.3 \ln\left(\frac{h/\hat{y}_r}{0.01}\right) \tag{31}$$

with

$$R_{01} = R[h/\hat{y}_r = 0.01].$$

Deviation from this straight line in a semi-logarithmic plot at high $h/\hat{y}_r$-ratios occurs at different values for different roughnesses.

8.2. *Annulus*

Experiments with ten different rough rods in four different smooth tubes, which are described and documented in [8] and [9], were re-evaluated. Except for the new equations for A_s and A_r, the transformation method used was that developed by Maubach [6] (setting $K_0 = 1.0$). The resulting R (h^+)-functions are similar to those in [8, 9]; the values of R for $h^+ = 150$ are shown in Fig. 24. The $h/\hat{y}_r$-effect on R is somewhat stronger than for the parallel-plate channel but weaker than that evaluated with a constant A_r.

For most roughnesses, the relation

$$R(150) = R_{01}(150) + 0.35 \ln\left(\frac{h/\hat{y}_r}{0.01}\right) \tag{32}$$

can be applied up to $h/\hat{y}_r = 0.1$ with an acceptable amount of scatter. The deviation from the straight line in the semi-logarithmic plot with increasing $h/\hat{y}_r$-ratios appears at smaller $h/\hat{y}_r (h/\hat{y}_r > 0.05)$ for roughnesses with narrow ribs (Nos 8, 9, 10) than for those with broad ribs (No. 4, and in the plane channel, $b/h = 2$). The difference in the variation of R with $h/\hat{y}_r$ is small

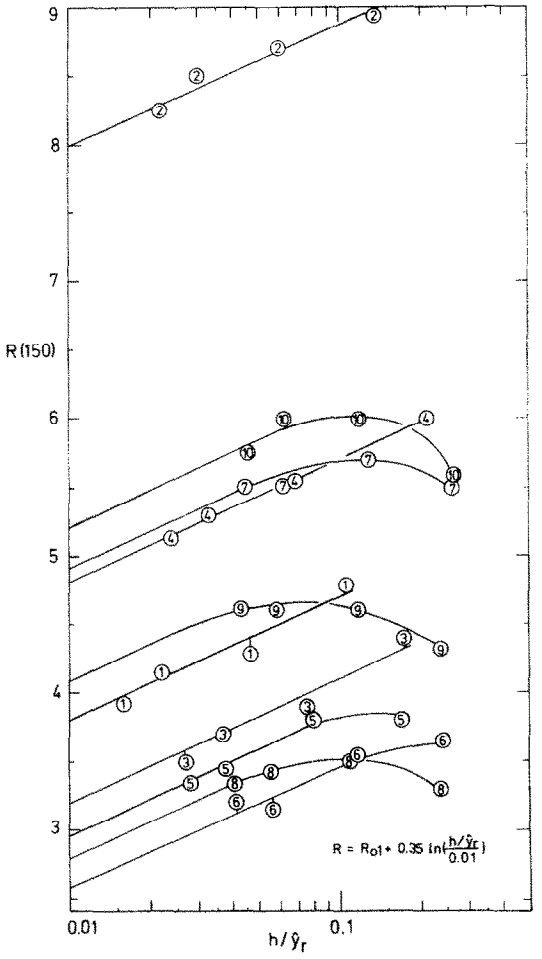

FIG. 24. The roughness parameter R in an annulus (for roughness geometry see Table 3).

between annulus and parallel plates, but because of the scatter of the data, it is not possible to decide conclusively whether this is a consequence of the curvature of the channel walls.

The accuracy of the determination of the zero shear stress line cannot be checked for the annulus experiment. The differences Δf in the rough zone friction factors obtained by the transformation method with constant A_r from [8, 9] and those obtained by the present method are shown in Table 3. The first value belongs to the lowest $h/\hat{y}_r$-ratio and the second to the highest $h/\hat{y}_r$-ratio being investigated. Negative values stand for smaller friction factors evaluated by the method with constant A_r. With the exception of No. 2 where $p/h = 61.5$, the difference Δf for low $h/\hat{y}_r$-ratios is less than $\pm 1\%$. For high $h/\hat{y}_r$-ratios, the new method yields up to 5.7% higher friction factors. These differences cannot be attributed to the new function for A_s, but are a consequence of the A_r value deviating from $A_r = 2.5$; this was checked by calculation. Differences due to the use of equation (27) for A_s rather than application of relation (6) of Warburton [10] are in the range $\pm 1\%$.

Table 3. Roughness geometry for experiments in annuli [8,9]; recalculated roughness parameter R_{01}; minimum and maximum differences in the rough zone friction factors obtained by the two transformation methods, i.e. with constant A_r, and with A_r given by equations (24) and (25)

No.	p/h	h/b	R_{01}	$\Delta f(\%)$	
1	6.25	0.96	3.8	−0.9	2.3
2	61.5	1.05	8.0	−2.5	1.6
3	4.06	1.64	3.2	−0.5	2.3
4	4.86	0.82	4.8	−1.1	2.0
5	5.77	1.73	3.0	0	3.5
6	4.08	2.61	2.6	0	3.5
7	4.07	0.98	4.9	−0.5	2.5
8	6.11	2.62	2.8	0.8	5.7
9	16.2	2.64	4.1	0.6	5.4
10	29.7	2.70	5.2	0.2	5.0

A compilation of R_{01} values is shown in Fig. 25, together with the function of Dalle Donne and Meyer, which was determined using a volumetric definition of the hydraulic diameter and the assumption that $A_r = 2.5$. For an exact determination of R as a function of the p/h- and b/h-ratios, more data must be evaluated.

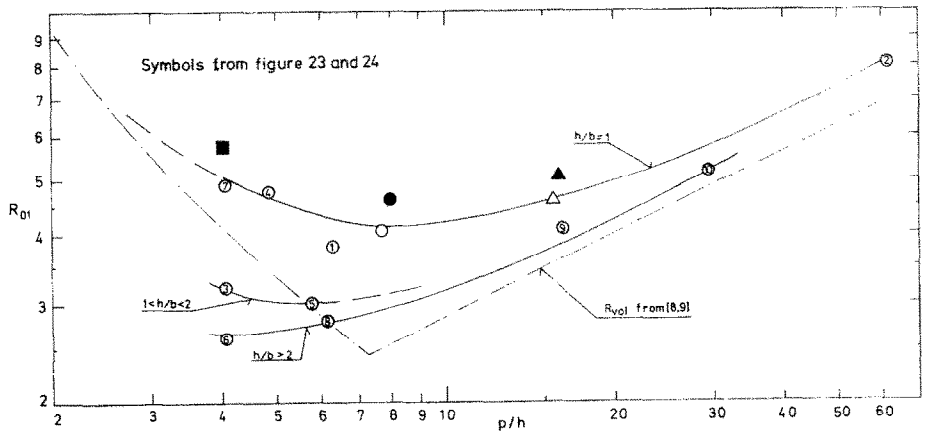

FIG. 25. The roughness parameter R_{01}.

9. CONCLUSION

The roughness parameter R cannot any longer be regarded as the only characteristic parameter for an artificial roughness. The slope A_r of the velocity profile is not constant but varies with the roughness and channel geometry.

In the use of logarithmic velocity profiles in a transformation method in order to locate the line of zero shear in an asymmetrical flow, the slopes determined by a best fit of the points lying on a straight line in a semi-logarithmic diagram cannot be employed; the deviation from a straight line, especially in the core flow, is too large. The experiments must be evaluated by an integral method in order to find velocity profile parameters which can be used in a transformation method. An important parameter in the analysis is the origin of the velocity profile at the rough wall. In order to get sensible functions for A_r and R, this origin should be defined quasi-volumetrically, i.e. eddy zones around the roughnesses should be treated as solid wall. If the profile parameters are determined in this way, it is found that the slope A_s of the velocity profile at the smooth wall decreases with increasing relative roughness height, normalized by the length of the smooth zone ($h/\hat{y}_s$). The slope A_r of the profile at the rough wall also decreases with increasing roughness height ($h/\hat{y}_r$). The extent of this deviation from the constant value of $A_r = 2.5$ depends on the friction factor of the roughness, being greater for roughnesses with high drag. The parameter R for a certain roughness is not constant either. It increases as the roughness height increases until some value of the $h/\hat{y}_r$-ratio, which depends on the drag of the relevant roughness-rib, is reached.

The description of flow in asymmetrical rough channels has become quite complex, but evaluations by a transformation method incorporating the new functions developed in the present work have resulted in friction factors of rough zones which differ by no more than 5.7% from previous results. For other than square two-dimensional roughnesses, the relations for the profile parameters have yet to be determined.

Acknowledgement—The author wishes to express his gratitude to Mr F. Merschroth for his help with the construction of the test rig and with the performance of experiments.

REFERENCES

1. W. B. Hall, Heat transfer in channels having rough and smooth surfaces, *J. Mech. Engng Sci* **4** (3), 287–291 (1962).
2. D. Wilkie, Calculation of heat transfer and flow resistance of rough and smooth surfaces contained in a single passage, *Proc. 3rd International Heat Transfer Conference, Chicago*, Vol. 1, pp. 20–31. A.I.Ch.E., New York (1966).
3. D. J. Nathan and M. A. M. Pirie, On the interpretation of heat transfer and pressure drop tests on roughened rods in smooth circular channels, C.E.G.B. Report RD/B/N 1370, Berkeley Nuclear Lab. (1970).
4. C. Warburton at ' M. A. M. Pirie, An improved method for analysing heat transfer and pressure drop tests on roughened rods in smooth channels, C.E.G.B. Report RD/B/N 2621, Berkeley Nuclear Lab. (1973).
5. J. Nikuradse, Strömungsgesetze in rauhen Rohren, *ForschHft. Ver. Dt. Ing.* 361 (1933), NACA TM 1292 (1950).
6. K. Maubach, Rough annulus pressure drop. Interpretation of experiments and recalculation for square ribs, *Int. J. Heat Mass Transfer* **15**, 2489–2498 (1972); see also: Reibungsgesetze turbulenter Strömungen, *Chemie-Ing.-Techn.* **42** (15), 995–1004 (1970).
7. W. Baumann and K. Rehme, Friction correlations for rectangular roughnesses, *Int. J. Heat Mass Transfer* **18**, 1189–1197 (1975).
8. M. Dalle Donne, Wärmeübertragung von rauhen Oberflächen, Kernforschungszentrum Karksruhe, KfK-Bericht 2397 (1977).
9. M. Dalle Donne and L. Meyer, Turbulent convective heat transfer from rough surfaces with two-dimensional rectangular ribs, *Int. J. Heat Mass Transfer* **20**, 583–620 (1977).
10. C. Warburton, Interpretation of tests on roughened pins in rough channels and the prediction of cluster pressure drop from single-pin data, C.E.G.B. Report RD/B/N 2930, Berkeley Nuclear Lab. (1974).
11. M. Bayazit, Free surface flow in a channel of large relative roughness, *J. Hydr. Res.* **14** (2), 115–126 (1976).
12. K. Hanjalic and B. E. Launder, Fully developed asymmetric flow in a plane channel, *J. Fluid Mech.* **51** (2), 301–335 (1972).
13. C. J. Lawn and M. J. Hamlin, Velocity measurements in roughened annuli, C.E.G.B. Report RD/B/N 1278 (1969).
14. C. J. Lawn, Flow measurements for establishing the mechanisms of heat transfer from a rib-roughened surface, C.E.G.B. Report RD/B/N 3514 (1976).
15. A. E. Perry and P. N. Joubert, Rough wall boundary layers in adverse pressure gradients, *J. Fluid Mech.* **17**, 193–211 (1963).
16. A. E. Perry, W. H. Schofield and P. N. Joubert, Rough wall turbulent boundary layers, *J. Fluid Mech.* **37**, 383–413 (1969).
17. C. K. Liu, S. J. Kline and J. P. Johnston, An experimental study of turbulent boundary layers on rough walls, Stanford University Report MD-15 (1966).
18. A. Aytekin and F. P. Berger, Turbulent flow in rectangular ducts with varying aspect ratios having one rough wall, NEA Coordinating Group on Gas Cooled Fast Reactor Development. Heat Transfer Specialist Meeting, Karlsruhe (1977).
19. A. W. Whitehead, The effect of surface roughening on fluid flow and heat transfer, Ph.D. Thesis, University of London (1976).
20. F. P. Berger and A. W. Whitehead, Fluid flow and heat transfer in tubes with internal square rib roughening, *J. Br. Nucl. Energy Soc.* **16** (2), 153–160 (1977).
21. W. Baumann, Geschwindigkeitsverteilung bei turbulenter Strömung an rauhen Wänden, Kernforschungszentrum Karlsruhe, KfK-Bericht 2618 and 2680 (1978).
22. Y. Furuya, M. Miyata and H. Fuijta, Turbulent boundary layer and flow resistance on plates roughened by wires, *Trans. ASME J. Fluids Engng* **98**, 635–644 (1976).
23. D. I. Kettle, The design of static and Pitot static tubes for subsonic speeds, *J. R. Aero. Soc.* **58**, 835–837 (1954).
24. F. A. MacMillan, Experiments on Pitot tubes in shear flow, ARC RM No. 3038, London (1956).
25. S. Goldstein, A note on the measurement of total head and static pressure in a turbulent stream, *Proc. R. Soc. London. Ser. A* **155**, 570–575 (1936).
26. J. O. Hinze, *Turbulence*. McGraw-Hill, New York (1959).
27. H. A. Becker and A. P. G. Brown, Response of Pitot probes in turbulent streams, *J. Fluid Mech.* **62**, 85–114 (1974).
28. V. C. Patel, Calibration of the Preston tube and limitation on its use in pressure gradients, *J. Fluid Mech.* **23** (1), 185–208 (1965).
29. H. C. Lavallee and A. T. Popovich, Fluid flow roughness

elements investigated by photolysis method, *Chem. Engng Sci* **29**, 49–59 (1974).
30. L. Meyer, Turbulente Strömung an Eizel- und Mehrfachrauhigkeiten im Plattenkanal, Kernforschungszentrum Karlsruhe, KfK-Bericht 2764 (1979) and Ph.D. thesis University Karlsruhe (1978).
31. L. Meyer, Flow resistance of rectangular roughnesses with varying density, OECD–NEA Coordinating Group on Gas Cooled Fast Reactor Development, Heat Transfer Specialist Meeting, Würenlingen, Switzerland (1979).

ECOULEMENT TURBULENT DANS UN CANAL RECTANGULAIRE A UNE OU DEUX PAROIS RUGEUSES

Résumé—L'hypothèse de profils de vitesse universels sur des surfaces lisses et rugueuses est largement utilisée pour le calcul de l'écoulement dans des canaux rugueux. On a réalisé des expériences dans un écoulement pleinement développé dans un canal rectangulaire d'un rapport variable de la hauteur à la largeur, afin de déterminer les paramètres des profils de vitesse sur des rugosités rectangulaires à deux dimensions. Dans des canaux rugueux à une et à deux parois rugeuses, on a mesuré les profils de pression et de vitesse en régime d'écoulement entièrement rugeux. Il en résulte que l'élévation du profil logarithmique sans dimension diminue dans les zones lisse et rugeuse avec l'augmentation de la hauteur relative de la rugosité et avec l'augmentation de la résistance de la rugosité, ce qui est en contradiction avec l'hypothèse généralement acceptée d'une élévation constante.

Les paramètres de profil déterminés sont décrits en fonction de la géométrie du canal et de la rugosité et introduits dans une méthode de transformation qui est appliquée à des données expérimentales obtenues par d'autres auteurs dans des canaux rectangulaires et annulaires.

TURBULENTE STRÖMUNG IN EINEM PLATTENKANAL MIT EIN- UND BEIDSEITIG RAUHEN WÄNDEN

Zusammenfassung—Für die Berechung der Strömung in rauhen Kanälen hat sich die Methode, die auf der Annahme universeller Geschwindigkeitsprofile über glatten und rauhen Oberflächen beruht, durchgesetzt. Es wurden Experimente in voll ausgebildeter Strömung in einem rechteckförmigen Kanal mit variablem Seitenverhältnis durchgeführt, um die Parameter der Geschwindigkeitprofile über zwei-dimensionalen rechteckigen Rauhigkeiten zu bestimmen. In ein- und beidseitig rauhem Kanal wurden Druck- und Geschwindigkeitprofile im vollrauhen Strömungszustand gemessen. Es zeigt sich, daß die Steigung des dimensionslosen logarithmischen Profils in der glatten und in der rauhen Zone mit wachsender relativer Rauhigkeitshöhe und wachsendem Widerstand der Rauhigkeit abnimmt, im Widerspruch mit der allgemein akzeptierten Annahme einer konstanten Steigung.

Die ermittelten Profilparameter werden als Funktion der Kanal- und Rauhigkeitsgeometrie beschrieben und in einer Transformationsmethode auf Experimente in Plattenkanälen und Ringspalten anderer Autoren angewandt.

ТУРБУЛЕНТНОЕ ТЕЧЕНИЕ В ПЛОСКОМ КАНАЛЕ С ОДНОСТОРОННЕЙ И ДВУСТОРОННЕЙ ШЕРОХОВАТОСТЬЮ СТЕНОК

Аннотация — При расчете течения в шероховатых каналах широко используется метод, основанный на предположении об универсальных профилях скорости над гладкими и шероховатыми поверхностями. Проводились опыты в условиях гидродинамической стабилизации в прямоугольном канале с переменным относительным размахом стенок канала с целью определения параметров профилей скорости над двумерными прямоугольными шероховатостями. В каналах с односторонней и двусторонней шероховатостью стенок измерялись профили напора и скорости течения в условиях развитой шероховатости. Оказывается, что наклон безразмерного логарифмического профиля в гладкой и шероховатой зонах уменьшается с ростом относительной высоты шероховатостей и повышением сопротивления шероховатой стенки, что противоречит общепринятому допущению о постоянном наклоне.

Полученные параметры профилей описываются в зависимости от геометрии канала и шероховатостей и в рамках метода преобразования применяются для обработки данных, полученных другими авторами в опытах с плоскими каналами и кольцевыми зазорами.